The Richness of the Dispersion Relation of Electromagnetic Bandgap Materials

Stefan Enoch, Gérard Tayeb, and Boris Gralak

Abstract—In this paper, we review several effects that arise from the richness of the dispersion relation of the electromagnetic bandgap materials (EBGMs). Indeed, EBGMs could simulate homogenous material whose optical index is lower than one or even negative (at least for the refraction). We take advantage of this property to design a lens with very short focal length or to confine emission in a narrow lobe. It is also shown how one can take advantage of the rapidly varying properties of the EBGMs near a band edge to design a prism whose dispersion is greater than any conventional prism or grating.

Index Terms—Electromagnetic bandgap materials (EBGMs), emission, refraction.

I. INTRODUCTION

ELECTROMAGNETIC bandgap materials (EBGMs) have been have been the subject of intensive research in the past few years. Basically, EBGMs are dielectric or metallic periodic structures whose spatial periods are of the order of magnitude of the considered wavelength. The unique feature of these structures is their ability to open a bandgap that is a frequency range for which the propagation of photons is forbidden whatever the direction of propagation and the polarization. A major consequence is the possibility to inhibit spontaneous emission that has been one of the earlier motivations to create photonic bandgaps [1].

In this paper, we will discuss some properties of the EBGMs when used with a wavelength that does not belong to the bandgap. We will review several effects and applications proposed by our group and others. Their common feature is that the key point is the richness of dispersion relation of EBGMs. Indeed, the bandgap is only one modification of the dispersion relation that follows from the periodic modulation of the permittivity of the structure. As a consequence, several effects have been demonstrated in recent studies such as superprism effect or negative refraction [2]–[4]

First, we will develop the theoretical tools we have used to understand and design the properties of EBGMs based devices. We will summarize the properties of the Bloch modes that propagate in infinite EBGMs and a special attention will be paid to the propagation of the energy.

Then we will apply these tools to design a EBGM that behaves as a homogeneous material with optical index smaller
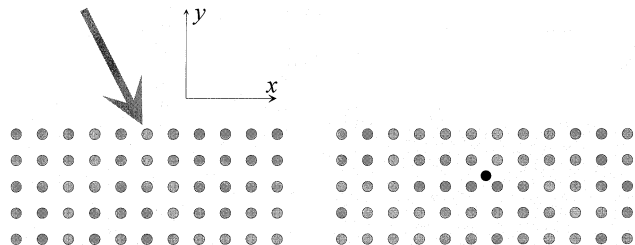
Fig. 1. Finite size 2-D EBGMs made of a finite number of rods. The structures could be illuminated by an external beam (left) of excited by an internal source (right). The coordinate system used in this paper is also represented.

than one (to illustrate ultrarefraction) or even with negative optical index (to illustrate negative refraction). An example of an ultrarefractive lens will be also given.

The shape of the dispersion relation at the vicinity of the band edge will allow us to design a prism whose dispersion is greater than any conventional prism or grating.

We will also show how to confine the emission of the light using a EBGM.

II. THEORETICAL TOOLS

We will consider throughout this paper two-dimensional (2-D) EBGMs made of a finite number of dielectric rods laying in vacuum. The rods are assumed to be infinite along the z axis (the coordinate system is defined on Fig. 1). We are interested in two situations: either the EBGM is enlightened by an external beam (or eventually a plane wave) or the EBGM is excited by an internal source, for example a dipole. In both cases, our aim is to predict the behavior of the finite structure from the knowledge of the properties of the infinite structure.

A. Infinite Structure

We have first to study the properties of the infinite structure. Thus, our objective is to find the allowed propagative modes in the structure and their properties. Of course, if there are no such propagative modes for a frequency range we have detected a bandgap.

Then we assume that the infinite structure fills the whole space and that there is no incident field. As we consider 2-D problems, two fundamental cases of polarization exist and all the following examples are for the E// case, that is when the electric field is parallel to the rods. The periods of the structure are $\mathbf{d}_1$ and $\mathbf{d}_2$ then for any integer values of l and m

$$\varepsilon(\mathbf{r} + l\mathbf{d}_1 + m\mathbf{d}_2) = \varepsilon(\mathbf{r}) \tag{1}$$

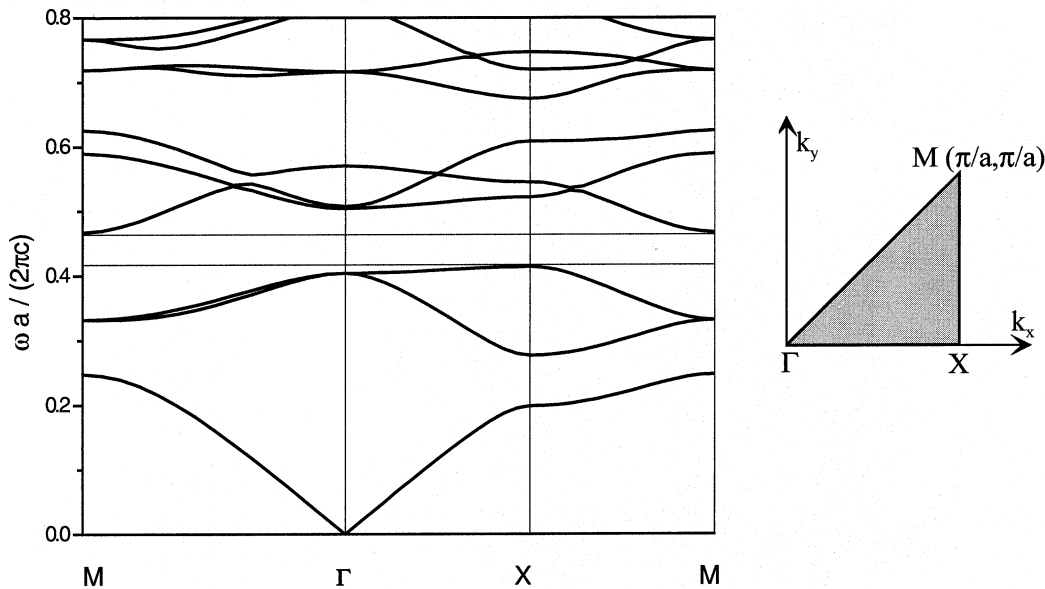where $\varepsilon(\mathbf{r})$ is the relative permittivity.

Fig. 2. Dispersion relation of the Bloch modes in a EBGM made of dielectric rods with permittivity $\varepsilon = 9$ lying in vacuum. The circular cross section of the rods has a radius $r = 0.475$. The rods are arranged on a square lattice with periods $a = d_1 = d_2 = 1.27$. The polarization is E// (the electric field is parallel to the rods). The small insert represents the reduced Brillouin zone.

It is now well known that the allowed propagative modes in EBGMs are Bloch modes (as for electrons in crystals). We assume a $\exp(-i\omega t)$ time dependence and use the usual complex amplitudes for harmonic fields. Thus, for any Bloch mode, the z-component of the electric field can be written in the form

$$u_{\mathbf{k}}(\mathbf{r}) = \exp(i\mathbf{k} \cdot \mathbf{r}) v(\mathbf{r}) \qquad (2)$$

where $v(\mathbf{r})$ is a periodic function

$$v(\mathbf{r} + l\mathbf{d}_1 + m\mathbf{d}_2) = v(\mathbf{r}) \qquad (3)$$

and $\mathbf{k}$ is the Bloch wave vector, which is usually assumed to be real.

It exists now several methods to calculate the dispersion relation $\omega(\mathbf{k})$ of the Bloch modes. Whatever the method used one can obtain a dispersion diagram usually represented as the one of Fig. 2 (the parameters of the structure are given in the figure caption). On this diagram, the normalized frequency $\omega a/(2\pi c) = a/\lambda(a = \|\mathbf{d}_1\| = \|\mathbf{d}_2\|)$ is represented as a function of the Bloch wave vector $\mathbf{k}$ whose extremity makes a path along the edges of the first reduced Brillouin zone. The first reduced Brillouin zone for the considered structure is represented in the insert of the Fig. 2.

For our purpose it is convenient to give a more complete representation of the dispersion relation as that shown on Fig. 3. Again the normalized frequency is plotted as a function of the Bloch wave vector, but now all the values of the first Brillouin zone are considered. The diagram on Fig. 2 is nothing else than the intersection between the sheets of Fig. 3 and vertical planes starting from the edges of the first reduced Brillouin zone (represented by the lines in the (k_x, k_y) plane).

We focus now on the frequency region just above the second bandgap. Fig. 4 is an enlarged view of the dispersion relation in
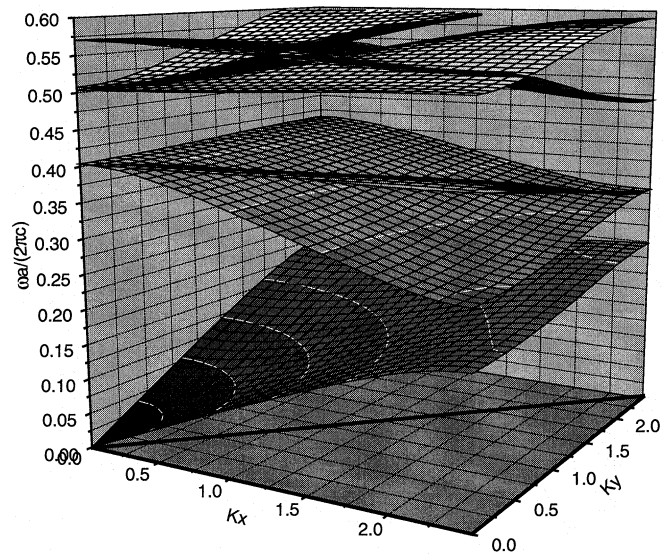

Fig. 3. 3-D dispersion diagram. The parameters are identical to those of Fig. 2. The lines in the (k_x, k_y) plane represent the first reduced Brillouin zone.

this region. Two bands represented by two sheets on this figure exist: an ascending one and a descending one when the Bloch wave vector components increase. Let us now consider a harmonic problem, that is to say a given frequency. The Bloch modes that can exist are given by the intersection of the sheets and a horizontal plane, for example the plane corresponding to the value $\lambda = 2.545$ of the limit between the two colors on the sheets on Fig. 4.

If we reproduce these intersections in the (k_x, k_y) plane and complete the diagram using the symmetries we obtain the constant frequency dispersion diagram of Fig. 5.

The last point concerns the direction of propagation of the energy of a given Bloch mode. On the diagram of Fig. 5 a given Bloch mode is represented by a point on the curves and it can be
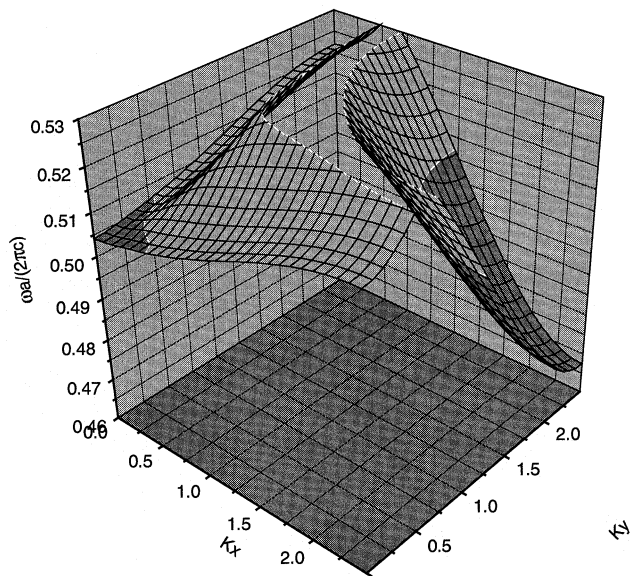
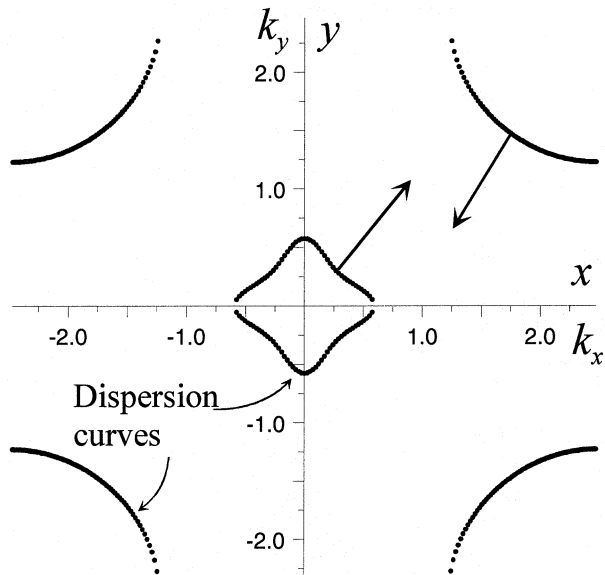Fig. 4. Enlarged view of the 3-D dispersion diagram of Fig. 3.

Fig. 5. Constant-frequency dispersion diagram for $\lambda = 2.545$. The arrows indicate the direction of the energy velocity for two particular Bloch waves.
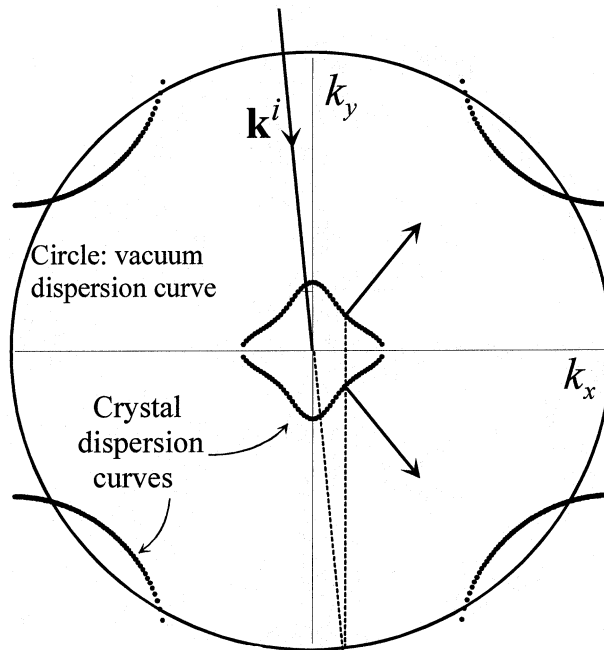

Fig. 6. Geometrical construction based on the conservation of the tangential components of the wave vector. The large circle with radius $k_0 = \omega/c$ represents the constant frequency dispersion diagram of vacuum. The angle of incidence of the plane wave is 6.4 degrees. (represented by the arrow coming from the top of the figure). The two Bloch modes that can be excited are deduced from the conservation of the tangential component of the wave vector (vertical dashed line). The arrows represent the direction of the associated energy flows.

shown that the average direction of propagation of the energy of this Bloch mode is given by the group velocity [9]

$$\mathbf{V}_g = \operatorname{grad}_{\mathbf{k}}(\omega). \tag{4}$$

On Fig. 5 the direction of $\mathbf{V}_g$ is perpendicular to the curves and points toward the ascending side of the sheets. Note that, of course, the direction of average phase velocity is given by $\mathbf{k}$ and his modulus is $\omega/\|\mathbf{k}\|$. Thus, it can be completely different from the group velocity.

B. Finite Size EBGMs

Now the question is: how can we use the dispersion relation of Bloch modes to predict or to design the properties of EBGM based devices.

The key point is that the tangential component of the Bloch wave vector is conserved at the boundaries of a slice of EBGM. This result is rigorously verified for an infinite slice of EBGM along the x axis [4].

Then we are led to the geometric construction shown on Fig. 6. The large circle is the constant frequency dispersion diagram of the surrounding media (with radius ω/c for example for the vacuum) while the other curves are the constant frequency dispersion diagram for the considered EBGM (identical to Fig. 5).

Let us consider that an incident plane wave illuminates a slice of this EBGM. We assume that the "interfaces" of the slice are perpendicular to the y axis. If the angle of incidence of the plane wave is such that its wave vector k^{i} is in the direction given by the solid line arrow (see Fig. 6), then the tangential component of this wave vector is given by the vertical dashed line. Thus, the two Bloch modes that can be excited in the structure are given by the intersection of this line and the constant frequency dispersion diagram. Given the ascending side of the corresponding sheets (see Fig. 4) the energy will flows toward the directions shown by the solid line arrows (starting form the dispersion curves).

Fig. 7 shows a map of the electric field modulus resulting from a rigorous numerical simulation using the extended Rayleigh method. A finite size EBGM made of 483 rods is enlightened by a limited beam coming from the top of the figure. The fringes above the structure are due to interferences between the incident beam and the reflected one on the first interface. The beam inside the EBGM propagates in the exact
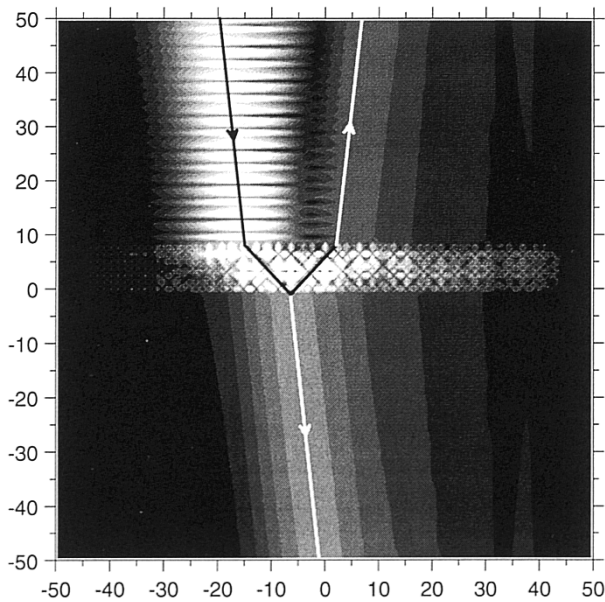
Fig. 7. Map of the electric field modulus for a EBGM made of 483 rods with the parameters of Fig. 2. The structure is illuminated by a gaussian beam with mean angle of incidence $\theta_0 = 6.4$ degrees. The lines show the locus of the maximum of the beams.
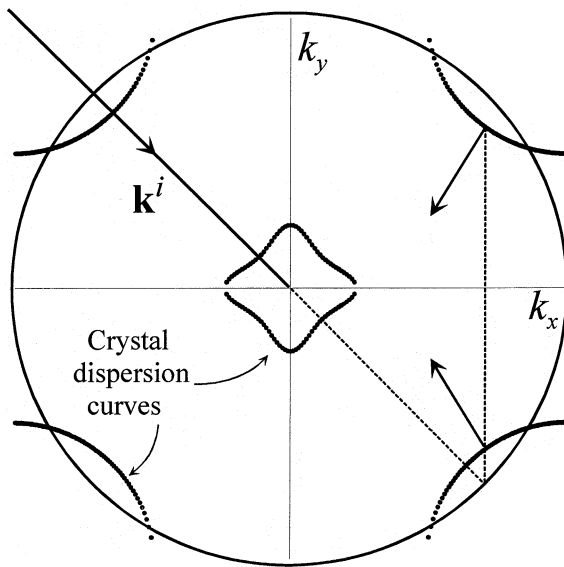

Fig. 8. Idem as Fig. 6 but with $\theta_0 = 40$ degrees.

Fig. 9. Idem as Fig. 7 but with $\theta_0 = 40$ degrees.

direction given by the previous geometrical construction. If we interpret this diagram in term of Snell–Descartes laws, it corresponds to an effective optical index smaller than one.

Let us now increase the angle of incidence such that the tangential component of the wave vector is given by the vertical dashed line on the Fig. 8. Then, the two Bloch modes that can be excited are given by the intersections with the constant frequency dispersion diagram, but now the ascending side of the sheets is toward the center of the figure (see Fig. 4) and the energy will propagate as represented by the arrows.

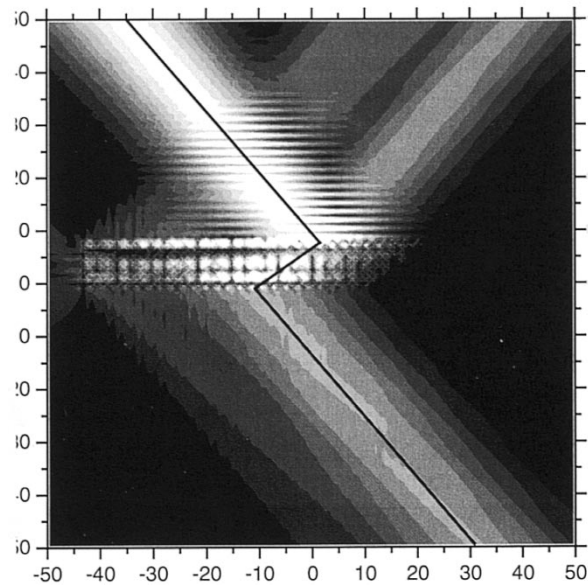Fig. 9 shows the electric field modulus map when a finite size EBGM is illuminated by a finite size beam and again

in the EBGM the energy propagates in the direction given by the geometrical construction. The refracted beam in the structure behaves as in a homogeneous media with negative optical index, which leads to call this phenomena "negative refraction."

Note that for these Bloch modes the average energy velocity is quasi-opposite to the average phase velocity and with a slight change of angle of incidence they can be exactly opposite. This remark and the fact that negative refraction can be observed makes the link with the so-called left-handed material or double negative material or also material with negative refractive index [11]–[15]. These materials are artificial materials that consist in periodic metallic structures (and can be also seen as a metallic EBGM). These structures are actually the subject of intensive research. Several properties such as their ability to focus even the evanescent waves to make a perfect lens have been studied [13]. Their realization in the optical domain will be difficult because of the losses of the metals for optical wavelengths. Here, the dielectric EBGMs could be a valuable alternative.

Note that the negative refraction has been experimentally observed in a very nice experiment by Kosaka *et al.* [3].

III. LENS

The first optical component we have tried to design was a lens, using a EBGM with effective index smaller than one (but positive) to obtain a lens with very small focal length. Usually, isotropic materials are used to design lenses. That is the reason why we have chosen the wavelength in order to obtain a constant frequency dispersion diagram that is almost a circle as represented on Fig. 10. Then the EBGM simulates a homogeneous isotropic material with very low effective optical index ($n_{\text{eff}} = 0.086$).

Fig. 10 shows the electric field modulus map when a EBGM that has been shaped with a quasi-circular interface is illuminated by a limited beam. A clear focusing of the light can be
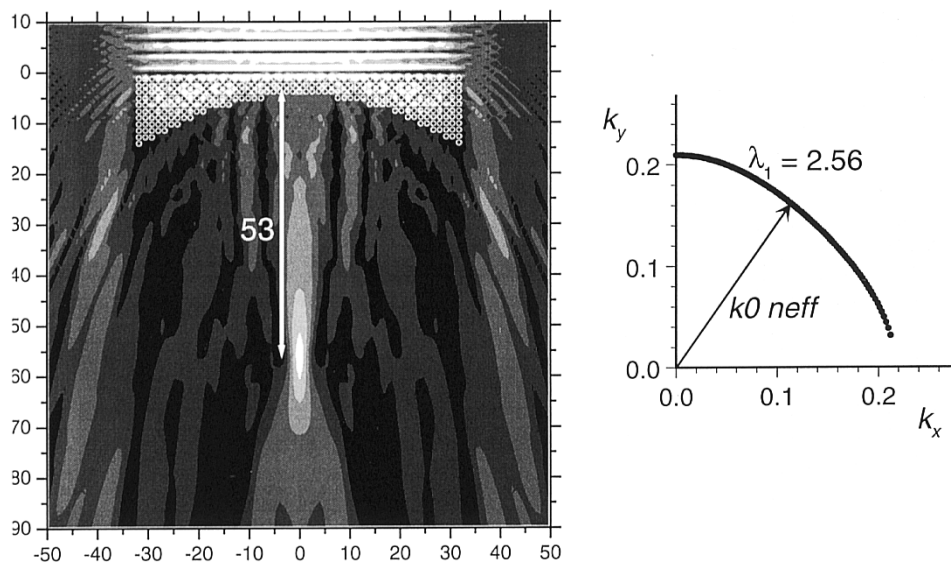
Fig. 10.   Left : micro-lens illuminated in normal incidence from the top by a Gaussian beam in E// polarization and with $\lambda = 2.56$. Right : constant frequency dispersion diagram for $\lambda = 2.56$.
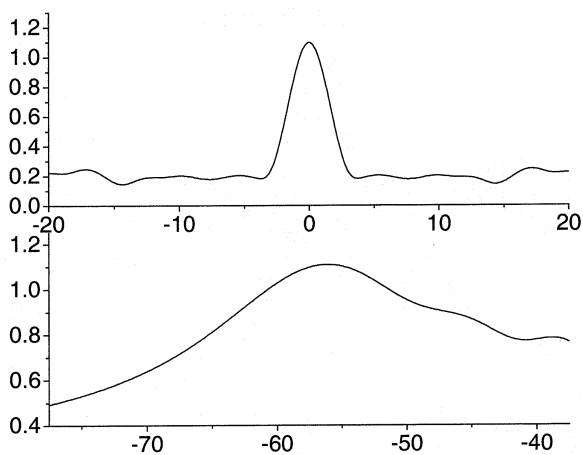

Fig. 11.   Modulus of the electric field. Top : along the x direction for $y = -57.5$. Bottom : along the y direction for $x = 0$.

observed. Note that a similar lens made with an ordinary dielectric would be a divergent lens. The focal length calculated using the classical formulas

$$f = \frac{R}{1 - n_{\text{eff}}} \qquad (5)$$

where R is the radius of the concave face of the lens, is equal to 55 (that is about 21 λ). This value is very close to the focal lens evaluated on the field map (about 53). In this example, the width of the lens is about 25 λ.

Fig. 11 shows the electric field modulus along x and y directions (through the focus point). The low level of the field modulus outside the focusing region along the x direction proves the focusing efficiency of the proposed lens.

In another connection, it has also been proposed by Luo *et al.* to design a lens using a slab of dielectric EBGM [16]. Their lens uses the negative refraction due to the fact that the constant frequency dispersion diagram at the considered wavelength is
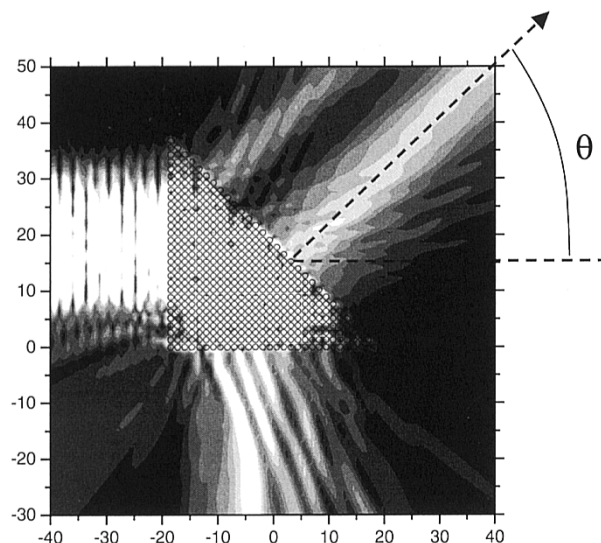

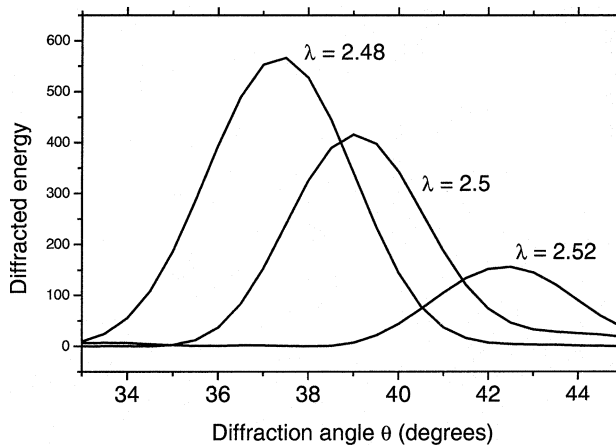Fig. 12.   Prism illuminated from the left by a Gaussian beam with $\lambda = 2.56$.

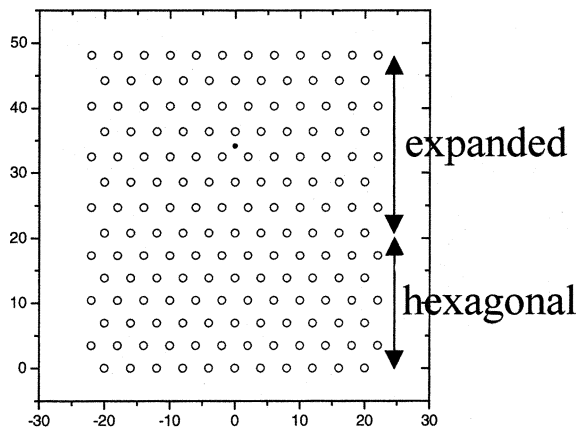Fig. 13.   Diffracted energy at infinity for three different wavelengths.

Fig. 14.   Structure made of a hexagonal EBGM and a vertically expanded structure. The source is located at $x_0 = 0$ and $y_0 = 34$. The dielectric circular rods with optical index 2.9 and radius 0.6 lie in vacuum. The period of the hexagonal lattice is $d = 4$. The expanded lattice is a hexagonal lattice expanded by a factor 1.127 in the y-axis direction.
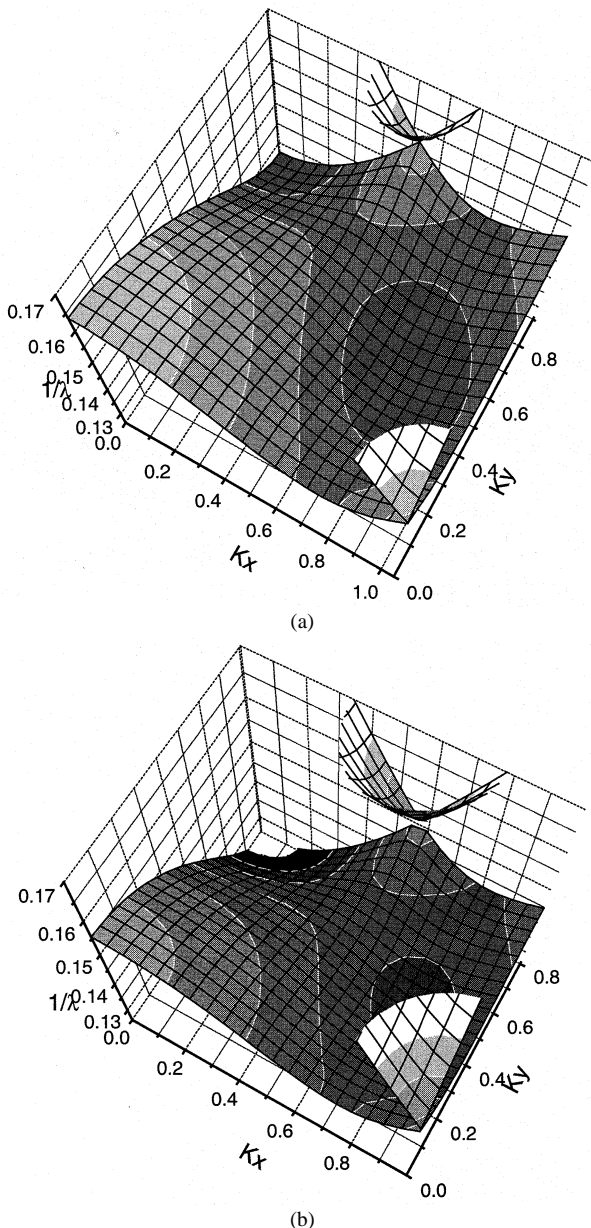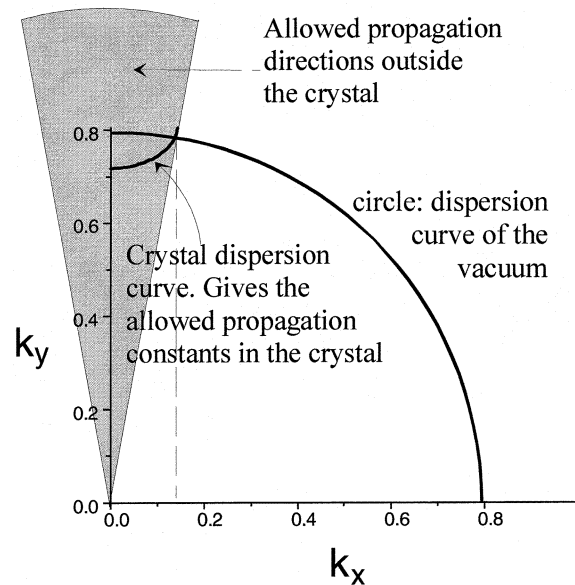

Fig. 16.   Schematic construction representing the conservation of the tangential component of the Bloch wave vectors.

convex. This lens is a potential alternative to the left-handed material based perfect lens, particularly in the optical domain where metals suffer from important losses.

IV. PRISM

When the wavelength is chosen close to the edge of the bandgap, one can take advantage of the parabolic shape of the dispersion relation. Indeed at the band edges the dispersion relation diagram has a horizontal tangent and then a small change of frequency can change significantly the properties of the EBGM. It has been proposed to design dispersive components [2].

On Fig. 12, a prism made of the same EBGM as previously is illuminated from the left of the figure by a beam and we look for the emerging beam from the larger edge of the prism. Note that the prism edge is only 14 λ. On Fig. 13 the far-field intensity is represented as a function of the angle θ for three slightly different wavelengths. The obtained prism is more dispersive than any usual prism or grating.

V. CONTROL OF THE EMISSION

Our aim is now to control the emission of a source embedded inside a EBGM. We will show how to canalize the emitted light in a narrow angular region outside the EBGM.

We consider a device made of two different EBGMs (see Fig. 14). One has a hexagonal lattice and the second has a lattice that is obtained by expanding the same hexagonal lattice in the y-axis direction. The excitation comes from a point source located roughly at the center of the expanded structure. The parameters are given in the figure caption.

Fig. 15 shows a part of the 3-D dispersion diagram for the two crystals and the lower horizontal plane of the figures has been chosen to correspond to the working wavelength of the source ($\lambda = 7.93$). For the hexagonal structure this wavelength is in the bandgap (there is no intersection between the sheets and the horizontal plane) while for the expanded structure solutions exist (in the upper left corner of the figure).

(a)

(b)

Fig. 15.   (a) Enlarged view of the 3-D dispersion diagram for the hexagonal structure. (b) Idem for the expanded structure.
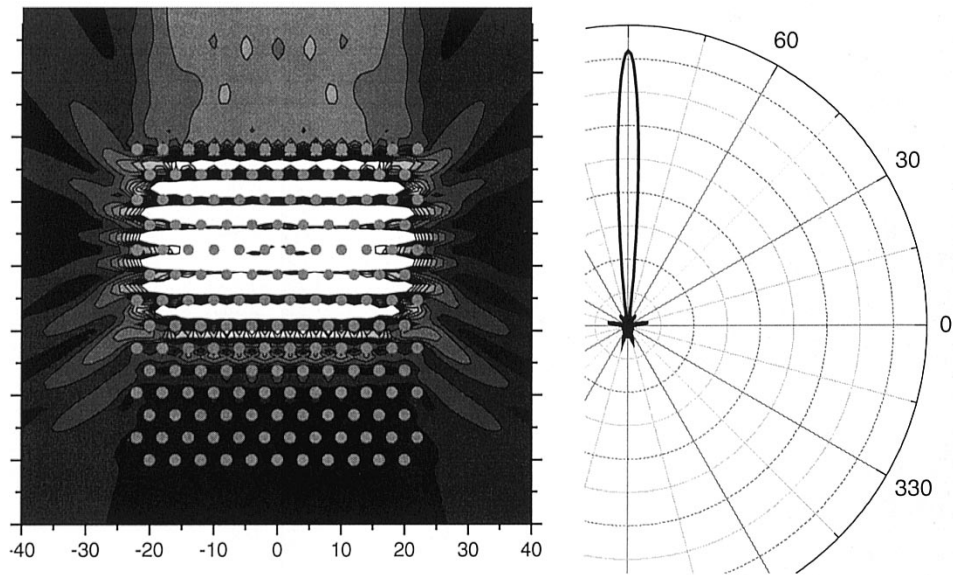
Fig. 17.   Left: electric field modulus radiated by the structure at $\lambda = 7.93$. Right: emission diagram.
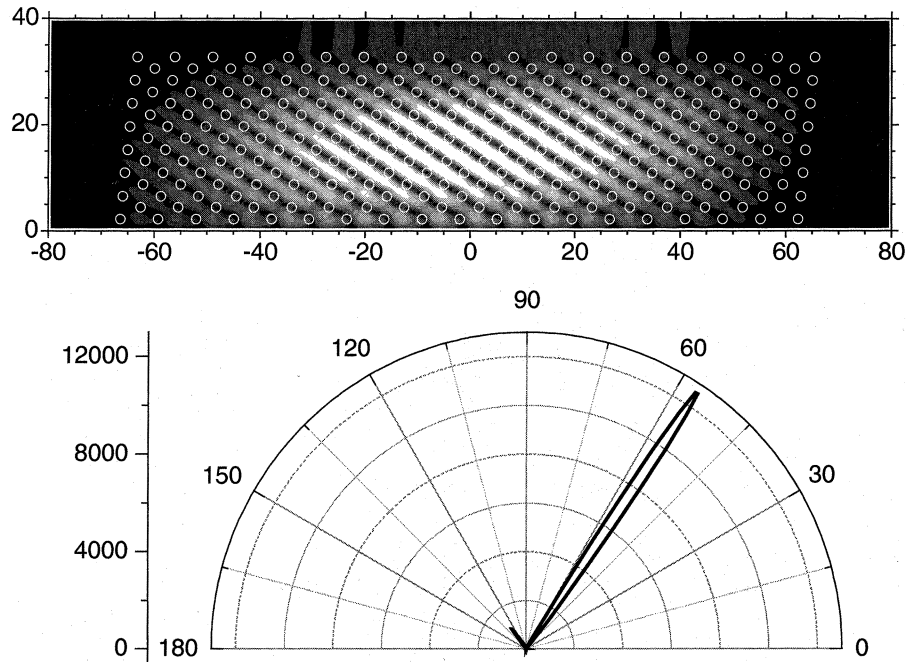

Fig. 18.   The structure has been expanded in a direction at 33 degrees. from the y axis and is above a ground plane. Top: electric field map when the structure is excited by a point source with $\lambda = 8.01$ located in the center of the structure. Bottom: emission diagram.

We assume that the source will emit in all the permitted modes and again we make use of the conservation of the tangential component of the wave vector. Fig. 16 shows the constant frequency dispersion diagram of the surrounding media (vacuum) and the expanded EBGM (the small ellipse-like curve). All the excited Bloch modes have their tangential component of the Bloch wave vector in the region delimited by the vertical dashed line. Thus, it must be the same for the waves excited in vacuum, that is to say that all the emitted light will be confined inside the gray angular domain and smaller is the ellipse smaller is these angular domain.

The field map (see Fig. 17) shows the electric field modulus when the structure is excited by a point source. The lower hexag-

onal structure prevents from the emission downwards. Note that the field fills the whole structure and that all the upper surface participates to the emission in vacuum. Here the important x-component of the phase velocity permits to obtain a surface that emits coherently.

The radiation pattern (Fig. 17) shows that the energy emitted from the EBGM source is canalized in a narrow lobe. As shown by Fig. 17, the emission from the lateral faces of the device is very low.

Fig. 18 shows another example that illustrates that we can design a source emitting in an off-axis direction by expanding the structure in a different direction. For this example the hexagonal structure has been replaced by an infinitely conducting ground

plane at $y = 0$. The radiation pattern shows clearly that the emission occurs principally in a lobe directed in a direction different from the normal to the mean out-coupling plane.

We have also studied the emission of dipoles in 3-D structures such as the so-called woodpile structure of simple cubic EBGMs and we have obtained an angular confinement of the emission together with an increase of the emitted power (and, thus, a decrease of the life time) [17], [18].

VI. CONCLUSION

In this paper we have shown that the modifications of the dispersion relation that comes from the periodic modulation of the permittivity leads to a rich variety of effects. Several effects such as negative refraction or control of the emission have been illustrated and fully understood using simple theoretical tools based on the dispersion relation of the Bloch modes in infinite EBGMs, and the continuity of the tangential component of the Bloch wave vector.

It must be reminded that the effects we have shown are due to a collective behavior of the whole EBGM and not to a local modification of the structure as in the case for example of a microcavity made by creating a defect in a EBGM. In that sense, the EBGMs can be considered as a metamaterial as the left-handed material are. One of the questions that has been raised is if the EBGMs could be an alternative to the left-handed materials for the optical wavelengths.

REFERENCES

[1] E. Yablonovitch, "Inhibited spontaneous emission in solid-states physics and electronics," *Phys. Rev. Lett.*, vol. 58, pp. 2059–2062, May 1987.
[2] S. Y. Lin, V. M. Hietala, L. Wang, and E. D. Jones, "Highly dispersive photonic band-gap prism," *Opt. Lett.*, vol. 21, pp. 1771–1773, Nov. 1996.
[3] H. Kosaka, T. Kawashima, A. Tomita, M. Notomi, T. Tamamura, T. Sato, and S. Kawakami, "Superprism phenomena in photonic crystals," *Phys. Rev. B*, vol. 58, pp. 10 096–10 099, Oct. 1998.
[4] B. Gralak, S. Enoch, and G. Tayeb, "Anomalous refractive properties of photonic crystals," *J. Opt. Soc. Amer. A*, vol. 17, pp. 1012–1020, June 2000.
[5] R. D. Meade, A. M. Rappe, K. D. Brommer, J. D. Joannopoulos, and O. L. Alerhand, "Accurate theoretical analysis of photonic band-gap material," *Phys. Rev. B*, vol. 48, pp. 8434–8437, Sept. 1993.
[6] A. Moroz, "Density-of-states calculations and multiple-scattering theory for photons," *Phys. Rev. B*, vol. 51, pp. 2068–20 817, Jan. 1995.
[7] N. A. Nicorovici, R. C. McPhedran, and L. C. Botten, "Photonic band gaps for arrays of perfectly conducting cylinders," *Phys. Rev. E*, vol. 52, pp. 1135–1145, July 1995.
[8] B. Gralak, S. Enoch, and G. Tayeb, "From scattering or impedance matrices to Bloch modes of photonic crystals," *J. Opt. Soc. Amer. A*, vol. 19, pp. 1547–1554, Aug. 2002.
[9] P. Yeh, "Electromagnetic propagation in birefringent layered media," *J. Opt. Soc. Amer.*, vol. 69, pp. 742–756, May 1979.
[10] D. Felbacq, G. Tayeb, and D. Maystre, "Scattering by a random set of parallel cylinders," *J. Opt. Soc. Amer. A*, vol. 11, pp. 2526–2538, Sept. 1994.
[11] V. G. Vesalgo, "The electrodynamics of substance with simultaneously negative values of ε and μ," *Soviet Phys. Uspekhi*, vol. 10, pp. 509–514, Jan. 1968.
[12] R. A. Shelby, D. R. Smith, and S. Schultz, "Experimental verification of negative index refraction," *Science*, vol. 292, pp. 77–79, Apr. 2001.
[13] J. B. Pendry, "Negative refraction makes a perfect lens," *Phys. Rev. Lett.*, vol. 85, pp. 3966–3969, Oct. 2000.
[14] R. W. Ziolkowski and E. Heyman, "Wave propagation in media having negative permittivity and permeability," *Phys. Rev. E*, vol. 64, pp. 56 625–1–56 625–15, Oct. 2001.
[15] A. Alu' and N. Engheta, "Anomalous mode coupling in guided-wave structures containing metamaterial with negative permittivity and permeability," in *Proc. 2002 2nd Conf. Nanotechnology*, Aug. 2002, pp. 233–234.
[16] C. Luo, S. G. Johnson, J. D. Joannopoulos, and J. B. Pendry, "All-angle negative refraction without negative effective index," *Phys. Rev. B*, vol. 65, pp. 201 104–1–201 104–4, May 2002.
[17] S. Enoch, B. Gralak, and Enoch, "Enhanced emission with angular confinement from photonic crystals," *Appl. Phys. Lett.*, vol. 81, pp. 1588–1590, Aug. 2002.
[18] S. Enoch, B. Gralak, and G. Tayeb, "Radiating dipoles in woodpile and simple cubic structures," in *Photonic Bandgap Material and Devices*, A. Adibi, A. Scherer, and S.-Y. Lin, Eds., 2002, vol. 4655, Proc. SPIE, pp. 241–250.

Stefan Enoch was born in Aix en Provence, France, on May 18, 1970. He was qualified from the École Nationale Supérieure de Physique de Marseille, France, in 1994. He received the Ph.D. degree in 1997. His thesis was on second-harmonic generation by gratings and rough surfaces.

He is currently a Researcher with the Fresnel Institute, Centre National de la Recherche Scientifique (CNRS), France. He is mainly involved in the theoretical and numerical study of photonic crystals.

Gérard Tayeb was born in Marseille, France, on November 11, 1959. He received the Agrégation of Physics in 1981 from the École Normale Supérieure de l'Enseignement Technique. He received the Ph.D. degree in 1990. His doctoral thesis dealt with diffraction by gratings, development of new methods, and application to anisotropic structures.

He joined the Laboratoire d'Optique Électromagnétique in 1985 (now in the Fresnel Institute). He is currently a Professor with the University of Aix-Marseille III. His research interests are in the investigation of photonic crystals properties.

Boris Gralak was born in Mont Saint Aignan, France, on January 16, 1975. He graduated from the École Polytechnique, Palaiseau, France, in 1997. He received the Ph.D. degree in 2001 from the Institut Fresnel, Marseille, France. His thesis dealt with theoretical and numerical studies of photonic bandgap materials, especially woodpile structures.

Since October 2001, he has been working as a Postdoctoral Researcher with FOM-Institute, Amsterdam, the Netherlands (AMOLF) where he is studying absorptive photonic crystals properties.